J Appl Electrochem (2014) 44:1025–1035
DOI 10.1007/s10800-014-0714-y

RESEARCH ARTICLE

Corrosion of the zinc negative electrode of zinc–cerium hybrid redox flow batteries in methanesulfonic acid

P. K. Leung · C. Ponce-de-León · F. J. Recio · P. Herrasti · F. C. Walsh

Received: 28 April 2014 / Accepted: 14 July 2014 / Published online: 17 August 2014

Abstract Corrosion of zinc in aqueous methanesulfonic acid has been evaluated over a wide range of concentrations of acid (0.5–5 mol dm^{-3}), dissolved zinc (0.5–2 mol dm^{-3}), and electrolyte temperature (22–50 °C). The corrosion rate of zinc, in terms of weight loss and the volume of hydrogen evolved, varied with time and it was found to be highly dependent on the surface state and electrolyte conditions. With an initial active layer of zinc present, the corrosion rate rapidly increased following a decline when the proton concentration in the solution decreased to ca. 0.56 mol dm^{-3}. Organic and inorganic inhibitors were added to the electrolyte to suppress the zinc corrosion in 1 mol dm^{-3} methanesulfonic acid. The strong adsorption and blocking effects of cationic organic adsorption inhibitors, such as cetyltrimethyl ammonium bromide and butyltriphenyl phosphonium chloride, led to a significant decrease in zinc corrosion over a 10 h immersion period. With the addition of indium and lead ions inhibitors, the zinc surface showed less activity. Zinc corrosion continued to a smaller extent in the presence of these metallic inhibitors during the first few hours, but the metallic layer of the inhibitors did not cover the surface completely resulting in continued hydrogen evolution and making the inhibitors less effective at longer times.

Keywords Butyltriphenyl phosphonium chloride · Corrosion · Cetyltrimethyl ammonium bromide · Hydrogen evolution · Indium · Inhibitors · Lead · Methanesulfonic acid · Zinc

List of symbols

A	Electrode area exposed to the electrolyte (m^2)
B	Constant in the Stern–Geary equation (V)
F	Faraday constant (C mol^{-1})
J	Current density (mA cm^{-2})
E_{cell}	Cell potential (V)
E_{cor}	Corrosion potential (V)
I_{cor}	Corrosion current (A)
j_{cor}	Corrosion current density (mA cm^{-2})
M	Molar mass of zinc (g mol^{-1})
R_p	Linear polarization area resistance (Ω cm^2)
z	Number of electrons involved in the reaction (dimensionless)
V_m	Molar volume of hydrogen under standard conditions (cm^3 mol^{-1})
V_i, V_0	Volume of hydrogen evolved in the presence, absence of corrosion inhibitor (cm^3)
β_a, β_c	Anodic, cathodic Tafel slope (V $decade^{-1}$)
Θ	Inhibition efficiency (dimensionless)

P. K. Leung · C. Ponce-de-León (✉) · F. C. Walsh
Electrochemical Engineering Laboratory, Energy Technology Research Group, University of Southampton, Highfield, Southampton SO17 1BJ, UK
e-mail: capla@soton.ac.uk

Present Address:
P. K. Leung
Instituto IMDEA Energía, Parque Tecnológico de Móstoles, Avda. Ramón de la Sagra, 3, E-28935 Móstoles, Madrid, Spain

F. J. Recio · P. Herrasti
Facultad de Ciencias, Departamento de Química-Física Aplicada, Universidad Autónoma de Madrid, 28049 Madrid, Spain

Present Address:
F. J. Recio
Departamento de Química de los Materiales, Facultad de Química y Biología, Universidad de Santiago de Chile, Casilla 40, Correo 33, 9170022 Santiago, Chile

1 Introduction

Zinc is commonly used as the negative electrode material in many modern energy storage devices, including primary and secondary batteries. Zinc is safe and easy to handle compared with lithium [1] and has the advantages of high specific energy density, generally lower cost, and widespread availability. These features make zinc very attractive for the use in large-scale energy storage systems. In the case of redox flow batteries [2], several systems, such as zinc–chlorine [3, 4], zinc–bromine [5, 6], zinc–air [7], and zinc–cerium [8, 9], have used zinc as a negative electrode in acidic media. The zinc–cerium flow battery [10] has been considered by research groups at the universities of Southampton [11–14] and Strathclyde [15, 16]. It realizes a relatively high open-circuit cell potential by combining the zinc half-cell with a Ce(IV)/Ce(III) redox half-cell, both electrolytes often being methanesulfonic acid based, and the cell is usually divided by a proton exchange membrane. The essential electrode reactions on charge are

$$\text{Negative electrode: } Zn^{2+} + 2e^- \xrightarrow{\text{charge}} Zn \qquad E^0 = -0.76\text{V vs. SHE} \tag{1}$$

$$\text{Positive electrode: } Ce^{3+} - e^- \xrightarrow{\text{charge}} Ce^{4+} \qquad E^0 = 1.28 - 1.72\text{V vs. SHE} \tag{2}$$

The desired cell reaction on charge is then

$$Zn^{2+} + 2Ce^{3+} \rightarrow Zn + 2Ce^{4+} \quad E_{\text{cell}} = 2.37\,\text{V} \tag{3}$$

During discharge, the reverse of reaction (3) is effective dissolution of zinc in the negative electrode compartment combined with reduction of Ce(IV) ions in the positive one. Since zinc is an active material, zinc dissolution and hydrogen evolution occur simultaneously in acidic electrolytes at open-circuit due to the following mixed electrode reactions on the zinc surface:

$$Zn - 2e^- \rightarrow Zn^{2+} \quad E^0 = -0.76\,\text{V vs. SHE} \tag{4}$$

$$2H^+ + 2e^- \rightarrow H_2 \quad E^0 = 0.\text{V vs. SHE} \tag{5}$$

Overall:

$$Zn + 2H^+ \rightarrow Zn^{2+} + H_2 \quad E_{\text{cell}} = 0.76\ \text{V vs. SHE} \tag{6}$$

Such corrosion leads to zinc wastage and decreases charge capacity and charge efficiency with the additional need to introduce hydrogen ventilation. There are few investigations on zinc dissolution in concentrated sulfuric [17], hydrochloric [18, 19], and phosphoric acids [20]. Recently, increasing attention has been given to the use of methanesulfonic acid in energy storage applications [3, 4, 7, 21]. This acid has advantages over other more conventional acids in terms of lower corrosivity, good ionic conductivity, and high solubility for common metal cations, such as Ce(III) [22], Pb(II) [23], and Ag(I) [24]. Additionally, zinc electrodeposition in methanesulfonic acid has been reported to have minimal dendritic growth after many hours of deposition [7, 11, 25]. Therefore, a longer battery cycle life can be achieved. In this work, zinc corrosion and hydrogen evolution have been investigated under a wide range of temperatures, zinc ion concentrations, and acidity levels. In addition, the corrosion of zinc was evaluated in the presence of various corrosion inhibitors.

2 Experimental

2.1 Chemicals and reagents

All chemicals were Analytical Reagent grade from Alfa Aesar and Sigma Aldrich. The electrolytes were prepared with ultrapure water (18 MΩ cm resistivity) from an Elga water purification system. Zn(II) methanesulfonate solutions were produced by stirring zinc carbonate basic (Alfa Aesar, UK, 99 wt%) using a PTFE-coated steel, magnetic stirrer follower (Fisherband, UK) in 99.8 % methanesulfonic acid (BASF, Germany). Zinc metal samples, 99.0 wt% were supplied by Rudgwick Metals, UK. The corrosion inhibitors, indium oxide, lead methanesulfonic, cetyltrimethyl ammonium bromide (CTAB), and butyltriphenyl phosphonium chloride were supplied by Sigma Aldrich AG (Germany), TIB Chemicals AG (Germany), and Fisher Scientific (UK), respectively.

2.2 Hydrogen evolution volume and zinc weight loss measurements

Measurement of hydrogen gas and weight loss of a metallic zinc sample was carried out in a calibrated 60 cm^3 polyethylene syringe (Plastipak Industries, Canada) as shown in Fig. 1a, in which a ≈3.5 g zinc sample was immersed in a controlled electrolyte composition at fixed temperature. The dimensions of the zinc samples were 2 cm × 2 cm × 0.15 cm and their surface was pre-treated by manually polishing with silicon carbide paper grade P120, degreasing with detergent (Teepol, UK), and etching in 30 vol% methanesulfonic acid for 20 s to obtain a light, matte, clean surface. Finally, ultrasonic cleaning for 1 min followed by rinsing with copious amounts of ultrapure water of 18 MΩ cm resistivity was used. The back surface and the edges of the zinc sample were covered with a polyester insulating tape (Cole-Parmer) to expose an active area of 4 cm^2. The weight of zinc was measured using an electronic balance with an accuracy of ±0.01 g (Scout Pro SP202, Ohaus, USA).

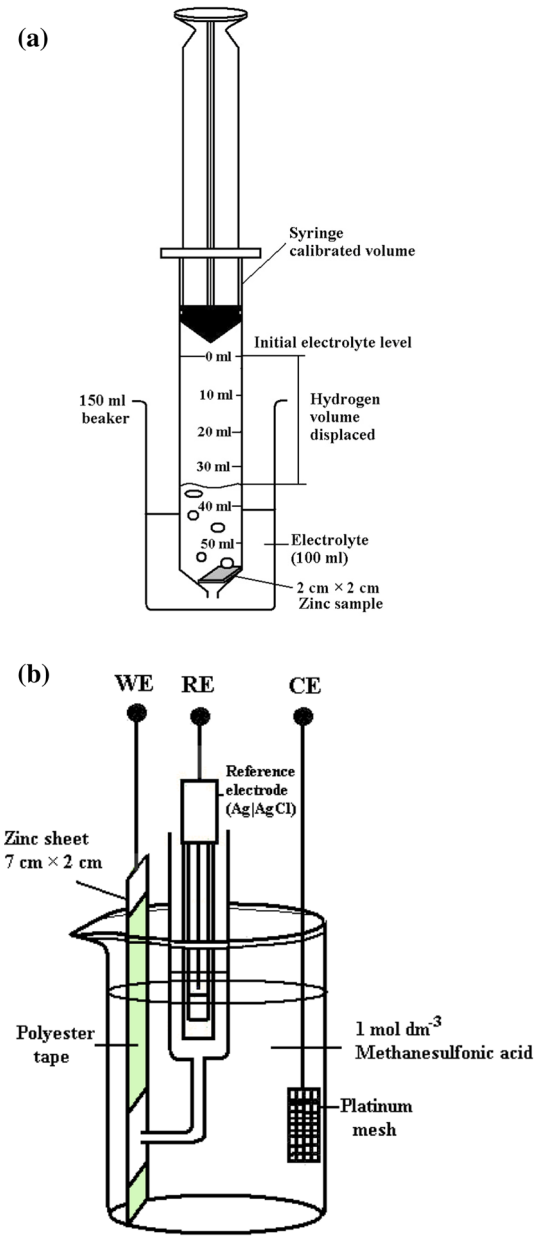

Fig. 1 The experimental arrangement used for **a** hydrogen collection and **b** potentiodynamic measurements

In order to measure the hydrogen evolved during zinc corrosion, the 60 cm^3 syringe was filled by pulling up 50 cm^3 of electrolyte from the beaker through the orifice at the bottom. The syringe was immersed in a beaker containing another 50 cm^3 of electrolyte as shown in Fig. 1a. When the zinc sample was exposed to the electrolyte, hydrogen evolves and displaces the solution contained inside the syringe indicating the volume of hydrogen generated by the corrosion reaction. The amount of hydrogen gas was recorded and the zinc sample was taken out to be weighed every 30 min. Once weighed, the zinc sheet was returned to the syringe and the electrolyte inside was replaced. The experimental procedures described above were repeated over a period of 10 h or until the zinc sample had completely dissolved.

2.3 Open-circuit electrode potential and potentiodynamic measurements

The open-circuit potential of the immersed zinc sample in 1 mol dm^{-3} methanesulfonic acid electrolyte in the presence and absence of a corrosion inhibitor was measured versus an Ag|AgCl reference electrode (ABB, Series 1400, 0.1 mol dm^{-3} KCl). The reference electrode communicated via a Luggin capillary, the tip being placed approximately 2 mm from the surface of the working electrode, in a 150 cm^3 glass beaker containing 100 cm^3 of electrolyte as shown in Fig. 1b. The dimensions of the zinc sample being tested were 7 cm × 2 cm × 0.15 cm and the sample was pre-treated as described in Sect. 2.2. The zinc sample working electrode was covered with an insulating polyester tape to ensure that the exposed area was 4 cm^2 (2 cm × 2 cm). The counter electrode was a platinum mesh of 1 cm^2 (1 cm × 1 cm).

Using the same experimental arrangement as above, the cathodic and anodic polarization measurements were carried out by linearly sweeping the potential of the zinc electrode at 2 mV s^{-1} using a computer controlled potentiostat (Metrohm Autolab BV, Netherlands). Each zinc sample was immersed in 1 mol dm^{-3} methanesulfonic acid at 22 °C and the polarization curves were used to characterize the surface condition. One zinc sample was used for the cathodic measurements with a fresh sample for the anodic measurements, each hour throughout a period of 10 h. The electrode potential was swept from the open-circuit potential up to 130 mV positive for the anodic polarization then 130 mV negative of the open-circuit value during the cathodic polarization measurements. The use of a sufficiently slow sweep rate facilitated steady-state current measurements. The specimen was analyzed by X-ray diffraction (XRD) using a Siemens D5000 X-ray diffractometer with Ni-filtered Cu K_α radiation ($\lambda = 1.5406$ Å).

3 Results and discussion

3.1 Corrosion of zinc in methanesulfonic acid

The open-circuit potential during the corrosion of zinc in methanesulfonic acid via hydrogen evolution

$$Zn + 2H^+ \rightarrow Zn^{2+} + H_2 \quad (7)$$

was studied by measuring both the zinc weight loss and the volume of the hydrogen gas evolved. Reaction (5) is

relatively fast in uncomplexing acid solutions and the exchange current density for hydrogen evolution is on the order of 10^{-8} mA cm^{-2} on zinc; both reactions (1) and (2) tend to be charge transfer controlled. From Faraday's law of electrolysis, the average rate of zinc weight loss assuming 100 % charge efficiency at a constant corrosion current, I_{cor} is given by

$$dw/dt = MI_{cor}/zF, \tag{8}$$

where M is the molar mass of zinc. Figure 2a illustrates the weight loss and the corresponding charge of a 3.5 g zinc sample (2 × 2 × 0.15 cm) over time when immersed in 1 mol dm^{-3} methanesulfonic acid. The sample was placed in two different solutions, 100 and 500 cm^3 volume. Zinc weight loss started slowly in the two solutions and increased almost at the same rate up to ≈1½ h. After 2 h, the dissolution rate increased steadily and leveled off after 6 h for the sample in the 100 cm^3 solution. The hydrogen evolution for this sample followed similar trend against time as it is shown in Fig. 2b. The volume of hydrogen is proportional to the mass of zinc dissolved in the electrolyte, according to Eq. (5); from Faraday's Law and the Ideal Gas Law, the volumetric rate of hydrogen production may be expressed as

$$\frac{dV}{dt} = \frac{V_m M A_j}{zF}, \tag{9}$$

where V_m is the molar volume of hydrogen under standard conditions. The mean volumetric rate of hydrogen evolution given by 1 g of dissolved zinc is equivalent to an electrical charge of 822 mA h and evolves 329 cm^3 of hydrogen (1 μA cm^{-2} = 2.92 mg dm^{-2} day^{-1} of Zn dissolution = 0.4 μL h^{-1} cm^{-2} of H_2 evolution at 25 °C) [26].

As shown in Fig. 2b, the estimated hydrogen volume based on the weight loss data is in agreement with the hydrogen volume observed experimentally during the zinc dissolution. Due to the limited electrolyte volume of 100 cm^3, the proton concentration decreased to ca. 0.31 mol dm^{-3} (Fig. 2b) after 10 h immersion. This decreasing of protons and the increased concentration of zinc ions in solution, due to the corrosion process, resulted in zinc dissolution stopping after approximately 6 h. When the zinc sample was immersed in 500 cm^3 of electrolyte, zinc corrosion took place at a steady rate as shown in Fig. 2a. This was due to the ability of the solution to maintain a high proton concentration (>0.6 mol dm^{-3}) indicating the importance of zinc ions and acid concentration in the electrolyte on the zinc corrosion.

Figure 2c illustrates the zinc dissolution rate and the zinc electrode potential versus time. The two curves follow a similar shape suggesting that the dissolution rate is related to the surface condition of the zinc sample. As soon

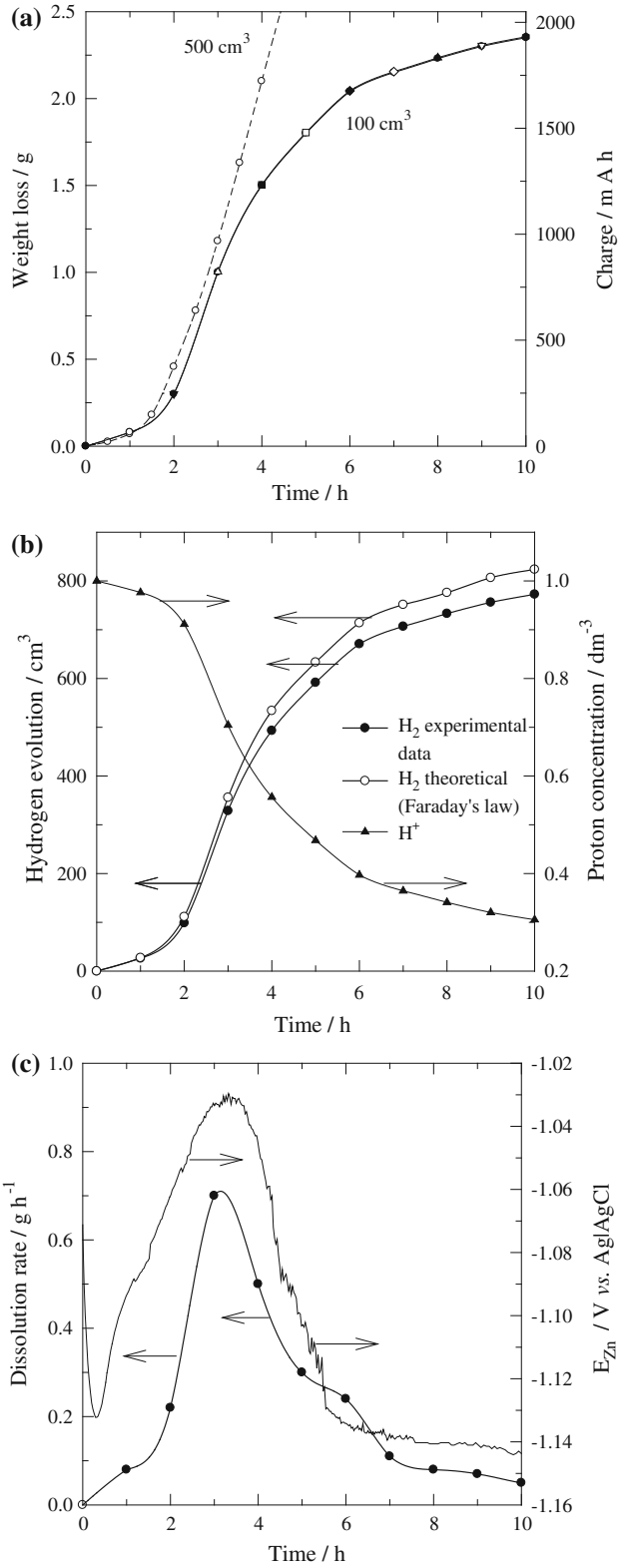

Fig. 2 Corrosion of zinc immersed in 1 mol dm^{-3} methanesulfonic acid for 10 h at 22 °C; as a function of **a** weight loss and charge density in electrolyte volume of 100 and 500 cm^3, **b** hydrogen evolution of the zinc plate, and **c** the zinc dissolution rate and its open-circuit half-cell potential

as the sample was immersed in solution, the electrode potential shifted toward negative values from −1.09 V versus Ag|AgCl to −1.13 V versus Ag|AgCl in the initial 20 min. The surface of the zinc sample changed from being exposed to the atmosphere (after etching) to the formation of an active corroded layer. During this first 20 min, the zinc dissolution increased up to 0.08 g h^{-1} followed by a rapid increase during the first 3 h of immersion. This observation is in agreement with the studies reported by Mouanga et al. [27] who measured zinc corrosion in 0.6 mol dm^{-3} NaCl. A chemical attack began when the active layer was formed within the first hour (20 min in this study). As in the previous literature, the active film in this test was black in color attributed to the small dispersed zinc particles as suggested by Feitnecht [28]. The increased surface area caused by the dispersed particles tends to reduce the hydrogen overpotential on the zinc surface [26]. During the formation of this film, the open-circuit potential increased from −1.13 to −1.03 V versus Ag|AgCl and the dissolution rate increased from 0.12 to 0.7 g h^{-1} in the third hour (Fig. 2c). The positive shift of the open-circuit potential is partly due to a higher zinc ion concentration in solution according to the Nernst equation:

$$E = E^0 - \frac{RT}{2F}\ln\left[Zn^{2+}\right] \quad (10)$$

The XRD pattern of a corroded zinc sample revealed that only metallic zinc was present after being immersed in 1 mol dm^{-3} CH_3SO_3H for 2 h. This agrees with the Pourbaix diagram that no oxide layer can be formed in the low pH media (pH < 7). The XRD data show the strongest diffraction peaks at 36.6°, 43.3°, and 70.1° (2θ), which represent preferential orientation along planes (002), (101), and (110), respectively [29, 30]. Using the Debye–Scherrer equation [31], the mean grain size was estimated to be 18 nm from the width of the strongest diffraction peak from the (101) plane.

Corrosion current densities and potentials were obtained from the polarization measurements at every hour throughout a 10 h immersion period as described in Sect. 2.3. At potentials close to the open-circuit corrosion (typically ±10 mV), linear polarization can be related to the corrosion current density, j_{cor} by the Stern–Geary equation, expressed as the area polarization resistance:

$$R_p = \Delta E/\Delta I = B/j_{cor}, \quad (11)$$

where B is the proportionality constant obtained from the cathodic, β_c, and anodic, β_a, Tafel slopes:

$$B = \beta_a\beta_c/2.3(\beta_a + \beta_c). \quad (12)$$

Figure 3a, b shows the logarithm of the current density versus the half-cell potential of zinc samples immersed in methanesulfonic acid at different times, i.e., for periods of

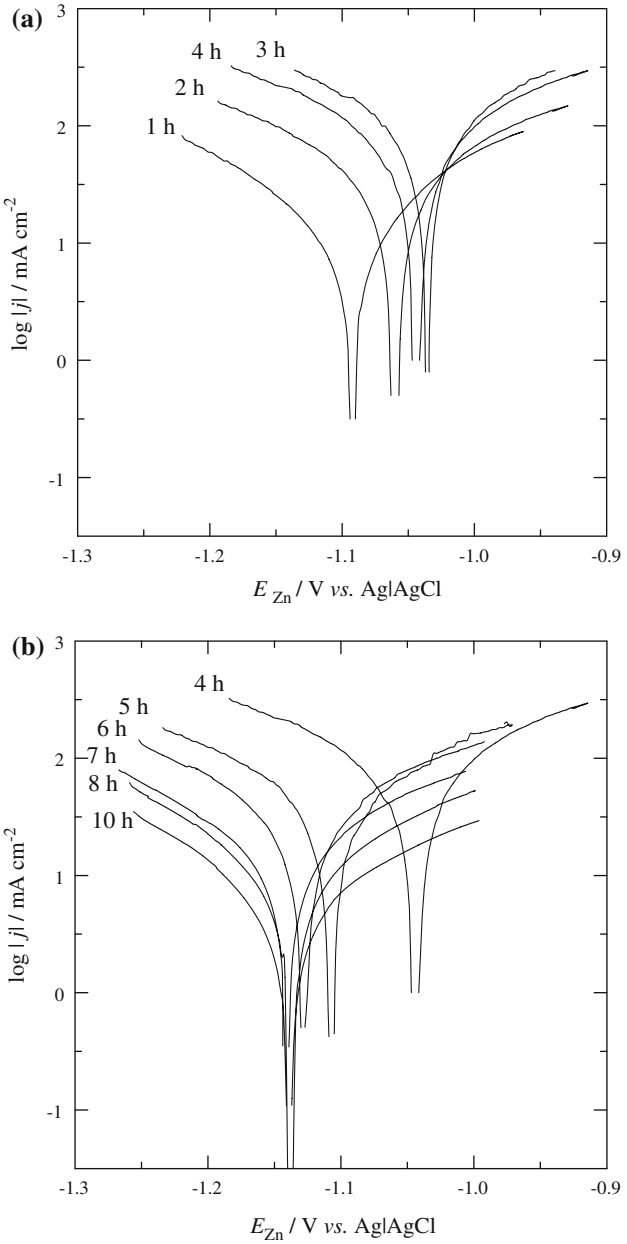

Fig. 3 Potentiodynamic polarization of zinc in 1 mol dm^{-3} methanesulfonic acid for the periods **a** 1st–4th hour and **b** 4th–10th hour. Sweep potential rate 2 mV s^{-1} at 22 °C

1–4 and 4–10 h, respectively. The cathodic, β_c, and anodic, β_a, Tafel gradients, corrosion current density, j_{cor}, corrosion potential, E_{cor}, and linear polarization area resistance, R_p, were calculated at each hour and reported in Table 1. Table also shows the comparison of the current density with that obtained from the weight loss experiments.

As shown in Table 1, corrosion current densities obtained from the Tafel plot were slightly lower than the averaged gravimetric values based on the weight loss measurements, although they both showed the same trend

Table 1 Electrochemical parameters for zinc dissolution from weight loss and polarization measurements at controlled times of immersion in 1 mol dm^{-3} methanesulfonic acid solution at 22 °C

Time, t (h)	Weight loss		Cathodic and anodic polarization				
	Weight loss rate (g h^{-1})	j (mA cm^{-2})	j_{cor} (mA cm^{-2}) (Tafel)	E_{cor} (V) vs. AglAgCl	$-\beta_c$ (mV $decade^{-1}$)	β_a (mV $decade^{-1}$)	R_p (Ω cm^2)
1	0.08	16.5	12	−1.09	165	143	0.69
2	0.22	45.0	38	−1.06	210	188	0.28
3	0.70	144.0	103	−1.04	165	184	0.09
4	0.50	103.0	79	−1.04	215	228	0.15
5	0.30	62.5	40	−1.11	230	206	0.30
6	0.24	49.5	28	−1.13	240	174	0.39
7	0.11	22.5	16	−1.14	210	155	0.60
8	0.08	16.5	13	−1.14	205	148	0.71
9	0.07	14.5	10	−1.14	199	140	0.88
10	0.05	10.5	6	−1.14	200	140	1.50

in corrosion evolution process. Such differences can be attributed to the resistance at the electrolyte/electrode interface and the charge used for the side reactions during the previous polarization measurement as reported in the literature [32–35]. Other possibilities such as local temperature and concentration of the electrolyte have also been discussed in detail by Zhang [26]. Another study reports that the corrosion current density increases as the zinc potential shifts in the cathodic direction during the active dissolution in 0.6 mol dm^{-3} sodium hydroxide [36]. This table shows that within the first 4 h the corrosion current density increased significantly up to 144.0 mA cm^{-2} and that the rate of zinc dissolution continuously decreased after this time together with the corrosion current densities. After immersing for more than 4 h, the proton concentration decreased and the zinc ion concentration increased due to the corrosion process resulting in the negative shift of the corrosion potential, which is consistent with the data presented in Fig. 2c. Since no decrease in current densities was observed when the zinc potential was swept toward the anodic direction in the Tafel plot as shown in Fig. 3a, b, there is no evidence of the formation of a passive oxide film.

After 7 h of immersion, the zinc weight loss rate remained less than 0.11 g h^{-1} and the open-circuit potential became steady at ca. −1.14 V versus AglAgCl. The general trend of zinc weight loss and its corresponding open-circuit potential during the 10 h immersion in methanesulfonic acid was similar in previous work reported by Stanojevic et al. [17] in sulfuric acid and Mouanga et al. [36] in sodium chloride solution.

3.2 Effect of methanesulfonic acid concentration

Figure 4a illustrates the average rate of zinc dissolution calculated by the weight loss at methanesulfonic acid concentrations from 0 to 12 mol dm^{-3} over a period of 10 h. The dissolution rate increased significantly with the concentration of acid reaching a maximum of ca. 3 g h^{-1} in 6 mol dm^{-3}. In the zinc–cerium flow battery developed by Plurion Inc. (UK), approximately 4.5 g of zinc deposit dissolved in the electrolyte after 2 h at open-circuit. The electrolyte composition was approximately at ca. 1.5 mol dm^{-3} Zn(II) methanesulfonate in 3 mol dm^{-3} methanesulfonic acid. The zinc dissolution rate was higher in this work due to the higher operating temperature at 60 °C [37].

The curve in Fig. 4a shows that the rate of zinc dissolution in methanesulfonic acid at concentrations higher than 6 mol dm^{-3} decreased due to the lower availability of dissociated hydrogen ions, H^+. High concentrated acid solutions are viscous and impractical for flow battery application since pumping costs are higher and the diffusion rate of electroactive species is lower. When the concentration of methanesulfonic acid is more practical, between 0.5 and 5.0 mol dm^{-3}, Fig. 4b shows the weight loss of zinc that has been exposed to different acid concentrations during the 10 h immersion. The curve shows that at methanesulfonic acid concentrations >3 mol dm^{-3} the weight loss is linear with time due to the large amount of protons in the electrolyte. In the case of acid concentrations higher than 1 mol dm^{-3}, the 3.5 g zinc sample still dissolves completely and only in the samples exposed to a lower acid concentrations some of the initial solid zinc remains after 10 h. The sample exposed to 0.5 mol dm^{-3} has similar behavior as in the 1 mol dm^{-3} acid. In the first hours, there is a moderate increase in zinc dissolution and hydrogen evolution and reaches a maximum rate after 6 h. Once the maximum had been achieved, the dissolution rate decreases due to the decrease in proton concentration and the increase in zinc ion concentration in the solutions. Similar results have been reported at comparable immersion times in 0.1–3.5 mol dm^{-3} hydrochloric acid [38]. The amount of

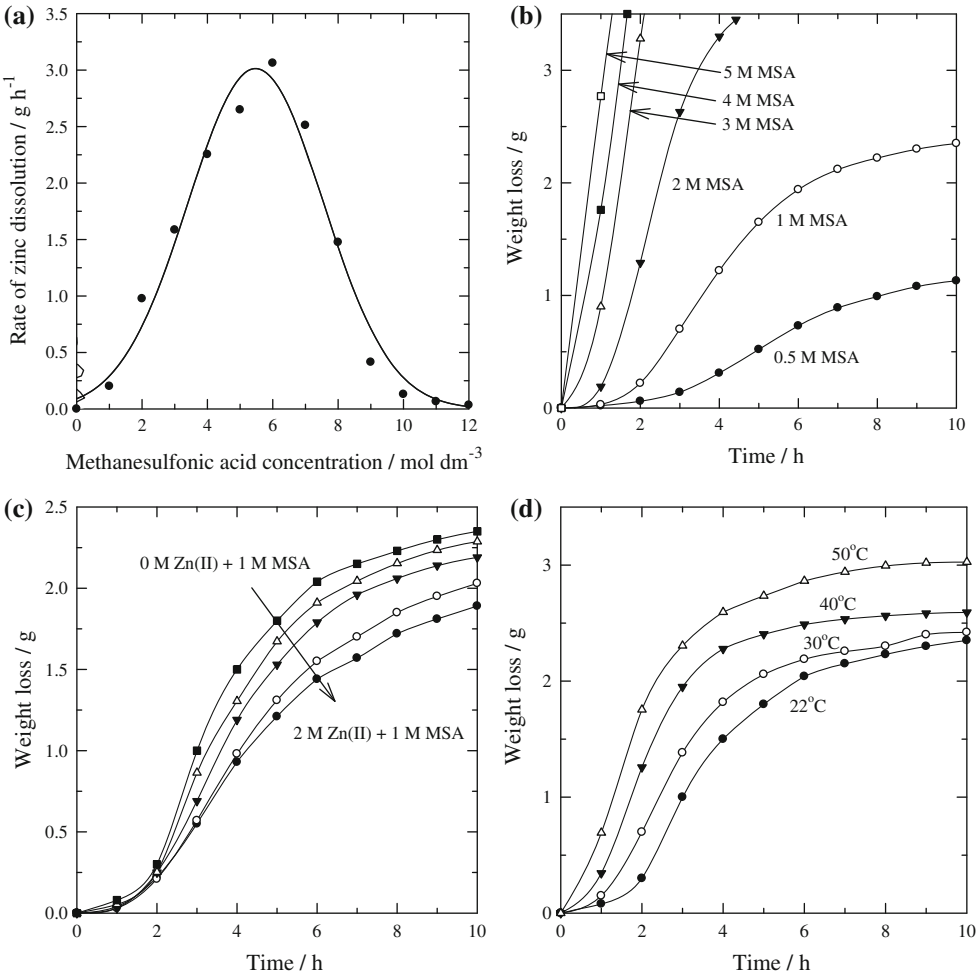

Fig. 4 Zinc corrosion in terms of weight loss in aqueous methanesulfonic acid solution. Rate of zinc dissolution in **a** 0–12 mol dm^{-3} acid, **b** 0.5–5.0 mol dm^{-3} acid, **c** 1 mol dm^{-3} acid with 0–2 mol dm^{-3} Zn(II), and **d** in 1 mol dm^{-3} methanesulfonic acid at temperatures of 22–50 °C

Table 2 The average corrosion rate of zinc in terms of weight loss and hydrogen evolution in various electrolyte compositions at temperatures of 22–50 °C

Methanesulfonic acid concentration (mol dm^{-3})	Zn(II) methanesulfonate concentration (mol dm^{-3})	Temperature (°C)	Corrosion current density, j_{cor} (mA cm^{-2})	Rate of zinc weight loss, dw/dt (g h^{-1})	Volumetric rate of hydrogen evolution, dV/dt (cm^3 h^{-1})
5	0	22	57.0	0.28	82.5
3	0	22	67.5	0.33	103.0
2	0	22	68.0	0.33	106.0
1	0	22	48.5	0.24	77.5
1	0.5	22	47.5	0.23	76.5
1	1	22	45.0	0.22	72.0
1	2	22	39.0	0.19	62.5
1	0	22	45.0	0.22	71.5
1	0	40	49.5	0.24	84.5
1	0	50	57.5	0.28	102.5

hydrogen evolution in this study has been summarized in Table 2 and the results are comparable to the theoretical conversion of weight loss, as discussed in Sect. 3.1.

The influence of the acid concentration in zinc corrosion has been evaluated by electrochemical techniques and by hydrogen volume measurements. The electrochemical measurements show current density values that are close to those calculated from zinc dissolution considering the amount of hydrogen evolved and the results obtained by weighting the amount of zinc during the experiments.

3.3 Effect of Zn(II) methanesulfonate concentration

Figure 4c shows the effect of the concentration of Zn(II) methanesulfonate, at a range of 0–2 mol dm^{-3}, on the weight loss of zinc when a zinc plate was immersed in solutions containing constant concentration of 1 mol dm^{-3} methanesulfonic acid for 10 h. Weight loss of zinc follows the same trend for all concentrations, in which the dissolution rate increases further after the second hour. The weight loss is lower as the concentration of Zn(II) ions increases and the zinc dissolution reaches a maximum at about 4 h. Table 2 also shows that the rates of zinc loss and hydrogen evolution were proportional to each other and decreased when the Zn(II) methanesulfonate concentrations increased. This confirms that the concentrations of Zn(II) and H^+ are important in controlling the rate of zinc dissolution.

The amount of zinc weight loss and hydrogen evolution decreased by ca. 20 % when the Zn(II) methanesulfonate concentration increased from 0 to 2 mol dm^{-3}. The reduced dissolution at higher zinc ion concentration has been reported in alkaline media [39–42]. In potassium hydroxide solution, Bockris [43] reported that the corrosion current density reduced to 1 μA cm^{-2} with the addition of 0.03–1 mol dm^{-3} zincate ions compared to 45 μA cm^{-2} in its absence. In the work of Meesus et al. [44], over 50 % of the hydrogen volume decreased by increasing the amount of zinc powder from 5 to 100 g in the electrolyte. Higher zinc ion concentration can be advantageous for rechargeable batteries as it allows the battery to charge at high current densities regardless of mass transport limitation and ensures that the Zn(II) species is present at all states of charge.

3.4 Effect of temperature

The zinc weight loss was investigated by immersing the zinc sample in 1 mol dm^{-3} methanesulfonic acid at 22, 30, 40, and 50 °C for a period of 10 h. The zinc corrosion rate increased rapidly at higher temperatures as indicated by the high rates of the zinc weight loss and the hydrogen evolution as summarized in Table 2. Figure 4d shows that the total weight loss of the zinc sample after immersion for 10 h was ca. 2.4 g at 22 °C but increased to ca. 3.0 g at 50 °C, in agreement with previous studies [40, 42, 45]. The higher zinc dissolution rate with temperature is attributable to the faster reaction kinetics at a higher temperature following the Einstein–Smoluchowski relationship and the increased mobility of protons in the solution. Since the total amount of hydrogen evolved, the depletion of proton concentration results in lower zinc dissolution rates at all temperatures after 4 h of immersion.

3.5 Effect of corrosion inhibitors

The relatively fast reaction of zinc corrosion in methanesulfonic acid suggests that it is crucial to add corrosion inhibitors in order to maintain the charge for a sufficient period of time after the battery has been charged. Four inhibitors were selected for this purpose: indium oxide, lead methanesulfonate, cetyltrimethyl ammonium bromide (CTAB), and butyltriphenyl phosphonium chloride. Previous studies [9, 46] have shown that they induce high overpotentials for the hydrogen evolution reaction [47, 48].

Figure 5a, b shows the effect of the four corrosion inhibitors on the open-circuit potential (OCP) of zinc and the hydrogen evolution respectively, versus time in 1 mol dm^{-3} methanesulfonic acid. The curves in Fig. 5a show that there are clear differences in the development of the OCP depending on the type of inhibitor used. In the case of metals, the OCP is similar to that without additive. The OCPs of the zinc sample with the addition of indium and lead were −1.12 and −1.11 V versus Ag|AgCl at the second hour of immersion, which were more negative than the one in the absence of inhibitor toward the anodic direction (−1.08 V vs. Ag|AgCl) during the formation of the black corroded zinc layer. These potential ranges are favorable for the deposition of a thin metallic layer of lead or indium on the zinc surface which is able to retard the start of the dissolution process. This layer is possible an incomplete monolayer and leaves only few active sites from which metallic zinc can be oxidized and might explain the previous stage before the increase of the dissolution rate where the rate remained low or constant for a short period of time. However, this stage always leads to an increase in the rate of dissolution of zinc which suggests that the disappearance or dissolution of the lead or indium layers is due to poor adhesion. Poor adhesion of the layer together with the surface being damaged by the hydrogen evolution on the uncovered sites would contribute to layer destruction and the high rate of zinc dissolution. Both figures indicate that lead (the more effective hydrogen poison) was protective than indium under the experimental conditions.

Organic additives, CTAB and butyltriphenyl phosphonium chloride, inhibit corrosion by adsorption on, and geometrically blocking of, the zinc surface [49, 50]. In the presence of such organic inhibitors, the OCPs of the zinc samples were more negative than that in the absence of inhibitor and shifted toward more positive values over time. In the presence of the inhibitors, zinc corrosion was inhibited effectively or temporarily, which was verified by the decrease in the hydrogen evolution rate and the corresponding weight loss rate (see conversion calculations in Sect. 3.1) as shown in Fig. 5b. With the addition of CTAB and butyltriphenyl phosphonium chloride, the total amount

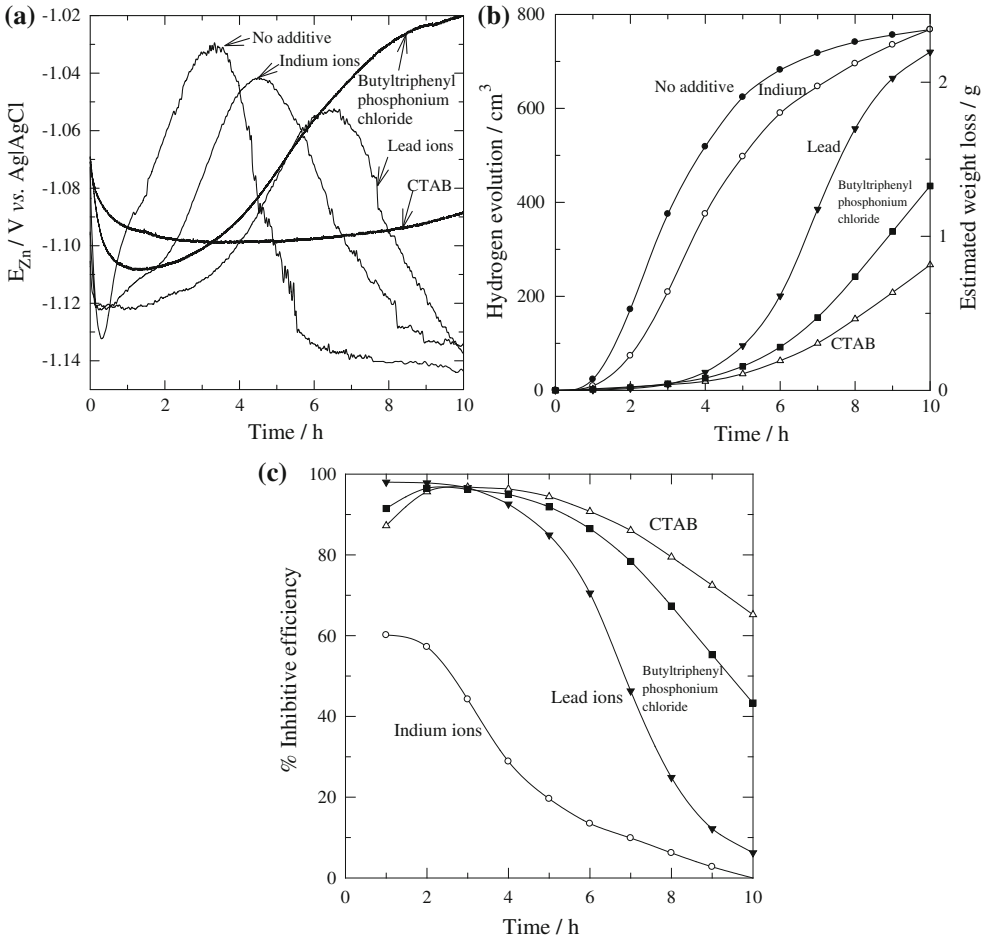

Fig. 5 The effect of the corrosion inhibitors indium oxide, lead methanesulfonate, CTAB, and butyltriphenyl phosphonium chloride at 2×10^{-3} mol dm^{-3} on **a** the zinc electrode potentials, **b** the volume of hydrogen evolution, the estimated weight loss, and **c** the inhibition efficiency

of hydrogen evolved was decreased significantly from ca. 800 cm^3 in the absence of inhibitor to around 200 cm^3 after 10 h of immersion. Although CTAB and butyltriphenyl phosphonium chloride have the advantages of superior inhibitive performance and lower toxicity, their strong adsorption and blocking effects may also inhibit zinc electrodeposition leading to a higher deposition overpotential and lower current efficiency [51, 52]. Since dendritic growth of zinc deposit is not significant in methanesulfonic acid as has been reported [7, 51], a high deposition overpotential is not favorable for battery applications and results in a lower voltage efficiency.

With the addition of lead ion inhibitor (lead methanesulfonate), the hydrogen evolution remained as low as 100 cm^3 after 5 h immersion compared to 600 cm^3 in its absence. Due to the formation of the metallic layers, the weight loss measurement of the zinc sample was no longer comparable to the hydrogen evolution data. The estimated weight loss of the zinc sample, Fig. 5b, was calculated using the charge density consumed according to the hydrogen evolution data as discussed in Sect. 3.1. Since the zinc OCP was more negative when the metallic layers of the hydrogen poisons indium and lead were formed on the zinc surface, such inorganic inhibitors served as cathodic inhibitors to slow down the corrosion rate. Despite this, the metallic layers formed were not completely covered on the zinc surface due to the continued hydrogen evolution during the process. Once the bare zinc was in contact with the solution, the zinc sample corroded instead of the less chemically active metallic coating of indium or lead and resulted in a sharp increase in hydrogen evolution as seen in Fig. 5b after the first and third hour. At later times, the zinc electrode potentials shifted toward more positive values, as shown in Fig. 5a, indicating the formation of the active layer.

After a sharp increase in the volume of hydrogen, the OCPs of the zinc sample stabilized in the fifth and seventh hours with the addition of indium or lead ions, respectively.

At that time, the total amount of hydrogen evolved was similar, approximately 500–600 cm^3, and the proton concentration in the electrolytes was depleted to about 0.5 mol dm^{-3}. This was indicated by the negative shift of the zinc electrode potential in Fig. 5a and the slowdown of the hydrogen evolution rate as shown in Fig. 5b. In the presence and absence of indium and lead compounds, the total amount of hydrogen evolved after 10 h of immersion was eventually similar (ca. 700 cm^3). Therefore, zinc corrosion cannot be inhibited with such inorganic inhibitors in the long term but can be effectively slowed down in the first few hours; lead inhibitor delayed the corrosion of zinc by nearly 3 h. The percentage inhibition efficiency, % *P,* can be calculated as

$$\% P = 100[1 - (V_i/V_0)], \quad (13)$$

where V_i and V_0 are the volumes of hydrogen evolution in the presence and absence of inhibitor, respectively. The curves in Fig. 5c show that the % *P* for all the inhibitors decreased with time. In the first 4 h, lead ion inhibited more than 90 % the evolution of hydrogen and dropped to less 6.2 % after 10 h immersion. The % *P* value for CTAB and butyltriphenyl phosphonium chloride was still over 40 % inhibition after 10 h.

4 Conclusions

1. The rate of zinc corrosion was highly dependent on the changes in surface condition during the process. The corroded zinc layer, which was black in color with a high surface area, formed after 20 min. The rate of zinc dissolution then increased significantly, while the corrosion rate decreased once the proton concentration dropped below ca. 0.56 mol dm^{-3}.
2. Zinc corrosion in terms of weight loss and hydrogen evolution increased significantly at lower Zn(II) methanesulfonate concentration, higher methanesulfonic acid concentration, and at elevated temperature.
3. The addition of CTAB and BTPC retarded significantly the rate of zinc corrosion with inhibition efficiencies >40 % after 10 h immersion in 1 mol dm^{-3} methanesulfonic acid. Despite this, the strong adsorption and blocking effects of such organic inhibitors may also inhibit the zinc electrodeposition process leading to higher deposition overpotentials during battery charging, resulting in lower voltage and current efficiencies.
4. Following the addition of inorganic indium or lead ions to the electrolyte, the metallic layers formed by indium oxide and lead methanesulfonate did not completely cover the zinc surface and some hydrogen evolution continued. Once bare zinc was in contact with the solution, zinc preferentially corroded instead of such metallic coatings resulting in fast dissolution. In the presence and absence of indium and lead compounds, the total amounts of hydrogen evolved after 10 h of immersion were similar. Therefore, zinc corrosion cannot be inhibited with such inorganic inhibitors in the long term but can be effectively slowed down in the first few hours.

Acknowledgments Financial support has been provided by the Research Institute for Industry (RIfI) at the University of Southampton. The authors are grateful to Drs. L. Berlouis and G. Nikiforidis, University of Strathclyde for helpful discussions and particularly appreciate the training in XRD provided by Dr. Mark Light. This work represents part of P.K. Leung's PhD research programme on the development of zinc-based flow batteries for energy storage and conversion technology.

References

1. Biensan Ph, Simon B, Pérès JP, Guibert A, Broussely M, Bodet JM, Perton F (1999) On safety of lithium-ion cells. J Power Source 81–82:906–912. doi:10.1016/S0378-7753(99)00135-4
2. Ponce de León C, Frías-Ferrer A, González-García J, Szánto DA, Walsh FC (2006) Redox flow cells for energy conversion. J Power Source 160:716–732. doi:10.1016/j.jpowsour.2006.02.095
3. Symons PC (1973) In: International conference on electrolytes for power sources. The Journal of The Electrochemical Society, Brighton
4. Symons PC (1970) Process for electrical energy using solid halogen hydrates. US Patent 3713888
5. Butler PC, Miller DW, Verardo AE (1982) In: 17th Intersocial Energy Conversion Engineering Conference, Los Angeles, USA
6. Lim HS, Lackner AM, Knechtli RC (1977) Zinc–bromine secondary battery. J Electrochem Soc 124:1154–1157. doi:10.1149/1.2133517
7. Clarke R (2009) Zinc air battery with acid electrolyte. US Patent 7582385, p B2
8. Clarke RL, Dougherty BJ, Harrison S, Millington JP, Mohanta S (2005) Battery with bifunctional electrolyte. US 2006/0063065A1
9. Clarke RL, Dougherty BJ, Harrison S, Millington JP, Mohanta S (2004) Cerium batteries. US Patent 2004/0202925A1
10. Walsh FC, Ponce de Léon C, Berlouis L, Nikiforidis G, Arenas-Martinez LF, Hodgson D, Hall D (2014) The development of Zn–Ce hybrid redox flow batteries for energy storage and their continuing challenges. ChemPlusChem (Submitted)
11. Leung PK, Low CTJ, Ponce de Leon C, Walsh FC (2011) Ce(III)/Ce(IV) in methanesulfonic acid as the positive half-cell of a redox flow battery. Electrochim Acta 56:2145–2153. doi:10.1016/j.electacta.2010.12.038
12. Leung PK, Low CTJ, Ponce de Leon C, Walsh FC (2011) Characterization of a zinc–cerium flow battery. J Power Source 196:5174–5185. doi:10.1016/j.jpowsour.2011.01.095
13. Leung PK, Ponce de Leon C, Walsh FC (2011) An undivided zinc–cerium redox flow battery operating at room temperature (295 K). Electrochem Commun 13:770–773. doi:10.1016/j.elecom.2011.04.011
14. Leung PK, Ponce de León C, Walsh FC (2012) The influence of operational parameters on the performance of an undivided zinc–cerium flow battery. Electrochim Acta 80:7–14. doi:10.1016/j.electacta.2012.06.074

15. Nikiforidis G, Berlouis L, Hall D, Hodgson D (2011) Evaluation of carbon composite materials for the negative electrode in the zinc–cerium redox flow cell. J Power Source 206:497–503. doi:10.1016/j.jpowsour.2011.01.036
16. Nikiforidis G, Berlouis L, Hall D, Hodgson D (2013) Impact of electrolyte composition on the performance of the zinc–cerium redox flow battery system. J Power Source 243:691–693. doi:10.1016/j.jpowsour.2013.06.045
17. Stajević D, Tošković D, Rajković MB (2005) Intensification of zinc dissolution process in sulphuric acid. J Min Metall B 41:47–66
18. Fouda AS, Madkour LH, EI-Shafel AA, Abd EIMaboud SA (1995) Corrosion inhibitors for zinc in 2 M HCl solution. Bull Korean Chem Soc 16:454–458
19. Abiola OK, James AO (2010) The effects of Aloe vera extract on corrosion and kinetics of corrosion process of zinc in HCl solution. Corros Sci 52:661–664. doi:10.1016/j.corsci.2009.10.026
20. Wang L, Pu JX, Luo HC (2003) Corrosion inhibition of zinc in phosphoric acid solution by 2-mercaptobenzimidazole. Corros Sci 45:677–683. doi:10.1016/S0010-938X(02)00145-2
21. Pan J, Sun Y, Cheng J, Wen Y, Yang Y, Wan P (2008) Study on a new single flow acid Cu–PbO_2 battery. Electrochem Commun 10:1226–1229. doi:10.1016/j.elecom.2008.06.008
22. Kreh RP, Spotnitz RM, Lundquist JT (1989) Mediated electrochemical synthesis of aromatic aldehydes, ketones, and quinones using ceric methanesulfonate. J Org Chem 54:1526–1531. doi:10.1021/jo00268a010
23. Hazza A, Pletcher D, Wills RGA (2004) A novel flow battery: a lead acid battery based on an electrolyte with soluble lead(II), Part I. Preliminary studies. Phys Chem Chem Phys 6:1773–1778. doi:10.1039/B401115E
24. Gernon MD, Wu M, Buszta T, Janney P (1999) Environmental benefits of methanesulfonic acid. Comparative properties and advantages. Green Chem 1:127–140. doi:10.1039/A900157C
25. Brodt G, Haas J, Hesse W, Jäqer HU (2003) Method for electrolytic galvanising using electrolytes containing alkane sulphonic acid. US 2003/0141195A1
26. Zhang XG (1996) Corrosion and electrochemistry of zinc. Plenum Press, New York. doi:10.1007/978-1-4757-9877-7
27. Mouanga M, Berçot P, Rauch JY (2010) Comparison of corrosion behaviour of zinc in NaCl and in NaOH solutions. Part I: corrosion layer characterization. Corros Sci 52:3984–3992. doi:10.1016/j.corsci.2010.08.003
28. Feitknecht W (1959) Studies on the influence of chemical factors on the corrosion of metals. Chem Ind 36:1102–1109
29. P.D.F.A. Index (1988) International Centre for Diffraction Data, Swarthmore, File4-831, ICDD
30. Gomes A, da Silva Pereira MI (2006) Pulsed electrodeposition of Zn in the presence of surfactants. Electrochim Acta 51:1342–1450. doi:10.1016/j.electacta.2005.06.023
31. Patterson AL (1939) The Scherrer formula for X-ray particle size determination. Phys Rev 56:978–986. doi:10.1103/PhysRev.56.978
32. Macias A, Andrade C (1987) Corrosion of galvanized steel reinforcements in alkaline solutions: Part 1: electrochemical results. Br Corros J 22:113–118. doi:10.1179/000705987798271631
33. Chang JC, Wei HH (1990) Electrochemical and Mössbauer studies of the corrosion behavior of electrodeposited FeZn alloys on steel. Corros Sci 30:831–837. doi:10.1016/0010-938X(90)90006-Q
34. Muralidharan VS, Rajagopalan KS (1978) Kinetics and mechanism of corrosion of zinc in sodium hydroxide solutions by steady-state and transient methods. J Electroanal Chem 94:21–36. doi:10.1016/S0022-0728(78)80395-7
35. Kear G, Walsh FC (2005) The characteristics of a true Tafel slope. Corros Mater 30:S1–S5
36. Mouanga M, Berçot P (2010) Comparison of corrosion behaviour of zinc in NaCl and in NaOH solutions; Part II: electrochemical analyses. Corros Sci 52:3993–4000. doi:10.1016/j.corsci.2010.08.018
37. Clarke RL, Dougherty B, Harrison S, Millington JP, Mohanta S (2004) Lanthanide batteries. USP 20040197651
38. Orubite-Okorosaye K, Oforka NC (2004) Corrosion inhibition of zinc in HCl using *Nypa fruticans* Wurmb extract and 1,5 diphenyl carbazonen. J Appl Sci Environ Manag 8:57–61
39. Snyder RN, Lander JJ (1965) Rate of hydrogen evolution of zinc electrodes in alkaline solutions. Electrochem Technol 3:161–166
40. Ruetschi P (1967) Solubility and diffusion of hydrogen in strong electrolytes and the generation and consumption of hydrogen in sealed primary batteries. J Electrochem Soc 114:301–305. doi:10.1149/1.2426582
41. Dirkse TP, Timmer R (1969) The corrosion of zinc in KOH solutions. J Electrochem Soc 116:162–165. doi:10.1149/1.2411786
42. Gregory DP, Jones PC, Redfearn DP (1972) The corrosion of zinc anodes in aqueous alkaline electrolytes. J Electrochem Soc 119:1288–1292. doi:10.1149/1.2403980
43. Bockris JOM, Nagy Z, Damjanovic A (1972) On the deposition and dissolution of zinc in alkaline solutions. J Electrochem Soc 119:285–295. doi:10.1149/1.2404188
44. Meeus ML, Strauven YAJ, Groothaert LAJ (1985) Zinc powder for alkaline batteries. European Patent Application, EP 161701 A1 19851121
45. Glaeser W, Künzel-Keune S, Merkel P (1999) The influence of discharge time on post-partial discharge gassing of zinc powder. J Power Source 80:72–77. doi:10.1016/S0378-7753(98)00252-3
46. Henriksen GL (1981) Zinc halogen battery electrolyte composition with lead additive. USP 4036003
47. Era A, Takehara Z, Yoshizawa S (1968) Influence of impurities especially lead contained in manganese dioxide upon the self-discharge of the Leclanche dry cell. Electrochim Acta 13:383–396. doi:10.1016/0013-4686(68)87010-0
48. Sato Y, Takahashi M, Assakura M, Yoshida H, Tada T, Kobayakawa K, Chiba N, Yoshida K (1992) Gas evolution behavior of Zn alloy powder in KOH solution. J Power Source 38:317–325. doi:10.1016/0378-7753(92)80121-Q
49. Zhu JL, Zhou YH, Gao CQ (1998) Influence of surfactants on electrochemical behavior of zinc electrodes in alkaline solution. J Power Source 72:231–235. doi:10.1016/S0378-7753(97)02705-5
50. Morad MS (2000) An electrochemical study on the inhibiting action of some organic phosphonium compounds on the corrosion of mild steel in aerated acid solutions. Corros Sci 42:1307–1326. doi:10.1016/S0010-938X(99)00138-9
51. Leung PK, Ponce de León C, Low CTJ, Walsh FC (2011) Zinc deposition and dissolution in methanesulfonic acid onto a carbon composite electrode as the negative electrode reactions in a hybrid redox flow battery. Electrochim Acta 56:6536–6546. doi:10.1016/j.electacta.2011.04.111
52. Shah MD, Panchal VA, Mudaliar GV, Shah NK (2011) Inhibitive effect of salicylidene-*N*-*N*′-dimorpholine towards corrosion of zinc in hydrochloric acid. Anti-Corros Methods Mater 58:125–130. doi:10.1108/00035591111130505